Symbol-Error Probabilities for Pulse-Position Modulation Signaling With an Avalanche Photodiode Receiver and Gaussian Thermal Noise

M. Srinivasan[1] and V. Vilnrotter[1]

The calculation of symbol-error probabilities for uncoded pulse-position modulation using a Webb-modeled avalanche photodiode receiver in the presence of additive Gaussian thermal noise is discussed. Performance curves for 256-ary pulse-position modulation obtained through Monte Carlo simulation as well as a numerical upper bound are presented. The Webb-plus-Gaussian model for the distribution of the received signal is compared with the much simpler Gaussian-only approximation. Results are presented for both fixed and optimized values of the avalanche photodiode gain parameter.

I. Introduction

The optical communication link currently under development for the X2000 program uses 256-ary pulse-position modulation (PPM) as the data modulation format. On the receiving end, an avalanche photodiode (APD) is used to detect the optical signal. The exact distribution of output electrons from the APD has been given in [1,2] but is cumbersome to use and may be approximated very closely by the Webb density function. In addition, the follow-on electronics contribute additive Gaussian thermal noise to the APD shot noise, resulting in an output that most accurately is modeled with a mixture density consisting of the convolution of discrete and continuous random variables. A simpler analysis involves modeling both APD shot noise and Gaussian thermal noise as a single Gaussian process. In [3], a comparison was made between these two approaches by calculating the resulting symbol-error probabilities for 4-ary PPM. In that article, it was shown that for very low levels of background radiation, the Gaussian approximation overestimates PPM symbol-error probability in the region $P_e < 0.01$. In this article, we perform the same comparison for 256-ary PPM using both numerical evaluation and Monte Carlo simulation. These results were compared with results obtained from the latest version of the Free-Space Optical Communications Analysis Software (FOCAS) program for optical communication link design,[2] which uses the Gaussian approximation. We show that in general the Gaussian approximation may either overpredict or underpredict symbol-error probability by varying degrees depending upon the levels of background and signal light levels. However, for the range of parameters relevant to the X2000

[1] Communications Systems and Research Section.

[2] M. Jeganathan and S. Mecherle, *FOCAS 2.0: Free-Space Optical Communications Analysis Software*, Optical Communications Group, Jet Propulsion Laboratory, Pasadena, California, May 1998.

project, the Gaussian approximation used by FOCAS is adequate for the high background-photon-level case without any adjustment factor. On the other hand, for low background-photon levels, the Gaussian approximation overpredicts symbol-error probability, and an adjustment of approximately 1 dB is called for. Finally, an upper bound on the error probability using the more accurate Webb-plus-Gaussian mixture density is calculated and proposed as a more uniform method of estimating PPM symbol-error probability.

II. APD Output Modeling

The average number of photons absorbed by an APD illuminated with total optical power $P(t)$ in T_s seconds can be expressed as

$$\bar{n} = \frac{\eta}{h\nu} \int_0^{T_s} P(t)dt \tag{1}$$

where h is Planck's constant, ν is the optical frequency, and η is the detector's quantum efficiency, defined as the ratio of absorbed to incident photons. The actual number of photons absorbed, n, is a Poisson distributed random variable with probability

$$p(n|\bar{n}) = \frac{\bar{n}^n}{n!} e^{-\bar{n}} \tag{2}$$

The conditional probability that an APD generates m electrons in response to exactly n absorbed photons, $m \geq n$, $n > 0$, has been shown by McIntyre to be [1]

$$p(m|n) = \frac{n\Gamma\left(\frac{m}{1-k}+1\right)}{m(m-n)!\Gamma\left(\frac{km}{1-k}+n+1\right)} \left[\frac{1+k(G-1)}{G}\right]^{n+km/(1-k)} \left[\frac{(1-k)(G-1)}{G}\right]^{m-n} \tag{3}$$

where G is the average APD gain and k is the ionization ratio. Averaging over the exact number of absorbed photons, we obtain

$$p(m|\bar{n}) = \sum_{n=1}^{m} p(m|n) \frac{\bar{n}^n}{n!} e^{-\bar{n}}, \qquad m \geq 1 \tag{4}$$

as the distribution of APD output electrons generated over T_s seconds given the mean number of absorbed photons in that interval. If no photons are absorbed, then no electrons can be generated according to this model. Conversely, no electrons are generated only if no photons have been absorbed. Hence,

$$p(m = 0|\bar{n}) = p(n = 0|\bar{n}) = e^{-\bar{n}} \tag{5}$$

An approximation to Eq. (4) has been derived by Webb [4] and provides a much simpler expression for the density of m in response to the mean number of photons absorbed:

$$p_w(m|\bar{n}) = \frac{1}{\sqrt{2\pi\bar{n}G^2F}\left(1+\dfrac{m-G\bar{n}}{\bar{n}GF/(F-1)}\right)^{3/2}} \exp\left(-\frac{(m-G\bar{n})^2}{2\bar{n}G^2F\left(1+\dfrac{m-G\bar{n}}{\bar{n}GF/(F-1)}\right)}\right) \tag{6}$$

where $F = kG + (2 - 1/G)(1 - k)$. This density is a continuous function that is defined for $m > -\lambda G/(F-1)$ and integrates to one in that range. The discrete probabilities in Eq. (4) are approximated by evaluating Eq. (6) at integer values of m. Note that Eq. (6) is defined for negative values of m, provided $m > -\lambda G/(F-1)$, even though negative m has no physical meaning. However, if the probability density function is summed over the non-negative integers, a value of less than one is obtained, as described in [5]. In the numerical evaluations presented here, we resolve this issue by calculating the sum of the Webb density values for $m \geq 1$ and assigning to $p(m = 0|\bar{n})$ the value of this sum subtracted from one. Incidentally, this method generally results in a closer approximation to the true distribution value at $m = 0$ given by Eq. (5) than does the value given by evaluating Eq. (6) at $m = 0$.

Added to the random number of APD output electrons is an independent Gaussian thermal noise charge from the follow-on electronics. The total charge then is integrated over each slot time T_s, resulting in a vector of Q independent observables for each received PPM word. It was proven in [6] that, given these observables, the maximum-likelihood detector structure consists of choosing the PPM symbol corresponding to the slot with the maximum accumulated charge value. If $\bar{n}_b$ and $\bar{n}_s$ are the mean number of absorbed background photons per slot and the mean number of absorbed signal photons per pulse, respectively, the Q-ary PPM symbol-error probability is

$$P_e(Q) = 1 - \int_{-\infty}^{\infty} p(x|\bar{n}_b + \bar{n}_s)\left[\int_{-\infty}^{x} p(y|\bar{n}_b)dy\right]^{Q-1} dx \tag{7}$$

where $p(x|\bar{n})$ is the probability density function for the slot statistic given $\bar{n}$ mean number of absorbed photons over the slot duration. Since the slot statistic is a random variable consisting of the sum of independent Webb and Gaussian random variables, its density function is the convolution of the individual densities and may be written as

$$p(x|\bar{n}) = \sum_{m=0}^{\infty} \phi(x, \mu_m, \sigma^2) p_w(m|\bar{n}) \tag{8}$$

where $\phi(x, \mu_m, \sigma^2)$ is the Gaussian density function with mean $\mu_m = mq + I_sT_s$ and variance $\sigma^2 = (2qI_s + [(4\kappa T)/R])\, BT_s^2$, as given in [3]. Here, q is the electron charge, κ is Boltzmann's constant, T is the equivalent noise temperature, B is the single-sided noise bandwidth, and I_s is the APD surface leakage current. Note that the APD surface leakage current is not multiplied by the APD gain and is modeled here as a constant DC current. The APD dark current, on the other hand, is multiplied by the APD gain and is modeled as part of the background radiation, i.e., it is incorporated into the value of $\bar{n}_b$.

An approach that sometimes is used to simplify calculation of PPM symbol-error probabilities is to model the density of the APD output electron charge as Gaussian with mean $qG\bar{n}$ and variance $q^2G^2F\bar{n}$. Then the slot statistic consisting of the sum of APD output electrons and amplifier thermal noise also is Gaussian and has mean $\mu = qG\bar{n} + I_sT_s$ and variance $\sigma^2 = \left[2q^2G^2F\bar{n} + qI_sT_s + ([4\kappa TT_s]/R)\right] BT_s$. Although simple, this approximation does not yield accurate results over all regions of interest, as previously shown in [3] and as we demonstrate here.

III. Calculation of Error Probabilities

Substituting Eq. (8) into Eq. (7), the PPM symbol-error probability may be expressed as [3]

$$P_e(Q) = 1 - \int_{-\infty}^{\infty} \sum_{m=0}^{\infty} \phi\left(x, \mu_m, \sigma^2\right) p_w\left(m|\bar{n}_b + \bar{n}_s\right) \left[\int_{-\infty}^{x} \sum_{n=0}^{\infty} \phi\left(y, \mu_n, \sigma^2\right) p_w\left(n|\bar{n}_b\right) dy\right]^{Q-1} dx$$

$$= \sum_{m=0}^{\infty} p_w\left(m|\bar{n}_b + \bar{n}_s\right) \int_{-\infty}^{\infty} \phi\left(x, \mu_m, \sigma^2\right) \left(1 - \left[\sum_{n=0}^{\infty} p_w\left(n|\bar{n}_b\right) \Phi\left(\frac{x-\mu_n}{\sigma}\right)\right]^{Q-1}\right) dx \tag{9}$$

where $\Phi(x)$ is the Gaussian distribution function $\Phi(x) = \int_{-\infty}^{x} (1/\sqrt{2\pi}) e^{-u^2/2} du$. The expression in Eq. (9) is difficult and time-consuming to evaluate accurately, so an upper bound is calculated instead. Although the union bound commonly is used for such Q-ary orthogonal signaling problems, a tighter bound was derived by Hughes [7] and is applied here. By observing that the function $f(u) = 1 - [1-u]^{Q-1}$ is concave for $u \in [0,1]$, Jensens's inequality gives us $E[f(u)] \leq f(E[u])$. Letting $u = \int_x^{\infty} p(y|\bar{n}_b) dy$ and taking the expectation over x with density function $p(x|\bar{n}_b + \bar{n}_s)$, we then can show that

$$P_e(Q) = \int_{-\infty}^{\infty} p\left(x|\bar{n}_b + \bar{n}_s\right) \left(1 - \left[\int_{-\infty}^{x} p(y|\bar{n}_b) dy\right]^{Q-1}\right) dx$$

$$= \int_{-\infty}^{\infty} p\left(x|\bar{n}_b + \bar{n}_s\right) \left(1 - \left[1 - \int_{x}^{\infty} p\left(y|\bar{n}_b\right) dy\right]^{Q-1}\right) dx$$

$$\leq 1 - \left[1 - \int_{-\infty}^{\infty} p\left(x|\bar{n}_b + \bar{n}_s\right) \int_{x}^{\infty} p\left(y|\bar{n}_b\right) dy dx\right]^{Q-1} \tag{10}$$

The double integral within the brackets on the right-hand side of Eq. (10) is simply the probability that a given background slot has a greater electron count than the signal-plus-background slot. This also may be interpreted as the symbol-error probability for equiprobable binary PPM signaling, denoted as $P_e(2)$, and given by

$$P_e(2) = \sum_{m=0}^{\infty} p_w\left(m|\bar{n}_b + \bar{n}_s\right) \int_{-\infty}^{\infty} \phi(x, \mu_m, \sigma^2) \sum_{n=0}^{\infty} p_w(n|\bar{n}_b) \Phi\left(-\frac{x-\mu_n}{\sigma}\right) dx \tag{11}$$

so that the upper bound on the Q-ary PPM symbol-error probability may now be expressed as $P_e(Q) \leq 1 - (1 - P_e(2))^{Q-1}$. In the numerical evaluation of Eq. (11), the infinite sums and integral are truncated to finite terms so that

$$P_e(2) = \sum_{m=0}^{M} p_w\left(m|\bar{n}_b + \bar{n}_s\right) \int_{A_m}^{B_m} \phi\left(x, \mu_m, \sigma^2\right) \sum_{n=0}^{N} p_w\left(n|\bar{n}_b\right) \Phi\left(-\frac{x-\mu_n}{\sigma}\right) dx + \epsilon \tag{12}$$

The limits M, N, A_m, and B_m are found by using the error bounds given in the Appendix of [3], resulting in truncation error ϵ.

Although the upper bound in Eq. (10) may be calculated relatively easily, it does require repeated evaluation of the Webb density and nested summation and integration. Use of the Gaussian approximation to the APD statistics saves computational time. Using this Gaussian approximation, the Q-ary PPM symbol-error probability is given by

$$P_{e,\text{Gaussian}}(Q) = \int_{-\infty}^{\infty} \phi\left(x, \mu_s, \sigma_s^2\right) \left[1 - \Phi\left(\frac{x - \mu_b}{\sigma_b}\right)^{Q-1}\right] dx \tag{13}$$

where $\mu_b = qG\bar{n}_b + I_s T_s$, $\mu_s = qG(\bar{n}_b + \bar{n}_s) + I_s T_s$, $\sigma_b^2 = \left[2q^2G^2F\bar{n}_b + qI_sT_s + ([4\kappa T T_s]/R)\right] BT_s$, and $\sigma_s^2 = \left[2q^2G^2F(\bar{n}_b + \bar{n}_s) + qI_sT_s + ([4\kappa T T_s]/R)\right] BT_s$ [3].

The two expressions for evaluating PPM symbol-error probability given in equations Eqs. (10) and (13) were calculated and compared using the following parameters, which were obtained from the FOCAS program: $Q = 256$, $T_s = 2 \times 10^{-8}$ seconds, $k = 0.007$, $I_s = 2 \times 10^{-9}$ amperes, $T = 300$ K, $R = 146,650\ \Omega$, and $B = 1/2T_s = 2.5 \times 10^7$ Hz ($1/2T_s$ is the noise equivalent bandwidth for an ideal integrator over duration T_s). Calculations were performed for several different values of $\bar{n}_b$ and $\bar{n}_s$. The APD gain parameter G was treated in two ways. In one set of calculations, it was held fixed at 40.0. In another set of calculations, G was optimized for each pair $\{\bar{n}_b, \bar{n}_s\}$ by taking on the value resulting in minimum PPM symbol-error probability. The fixed-gain results may be used to indicate the sensitivity of the system to mismatch between the fixed-gain value and the optimal-gain value under actual operating conditions. In addition to numerical evaluation, because the expression given in Eq. (10) is an upper bound, Monte Carlo simulations of the receiver performance under the Webb model also were performed in order to obtain more accurate results for lower signal-to-noise ratio (SNR) regions. In the Monte Carlo simulations, the Webb deviates needed to simulate APD output were generated using the inclusion–exclusion principle [8] following the method outlined in [9].

The results for G fixed at 40.0 are presented first. This value of G was obtained by using the FOCAS program, which approximated it to be the gain value that maximizes the signal-to-noise ratio for $\bar{n}_b = 150$ and $\bar{n}_s = 70$ and the parameters given previously, corresponding to daylight operating conditions. For this maximization, the SNR is defined in FOCAS[3] as

$$\text{SNR} = \frac{\bar{n}_s^2}{F(\bar{n}_s + \bar{n}_b) + n_{ds} + n_t} \tag{14}$$

where bulk dark current electrons have been incorporated into $\bar{n}_b$, $n_{ds} = I_s T_s / qG^2$ is the surface leakage current electron count, and $n_t = (\text{NEI})^2 T_s / 2q^2G^2$ is the electron count from the amplifier noise equivalent current, which is given by $\text{NEI} = \sqrt{4\kappa T/R}$.

Figures 1 through 5 show plots of P_e versus $\bar{n}_s$ for various values of $\bar{n}_b$. The three curves shown are the error probability for the Webb model obtained through Monte Carlo simulation, the upper bound for the Webb model as given by Eq. (10), and the error probability for the Gaussian approximation as given by Eq. (13). From these figures, we see that the upper bound, Eq. (10), approaches the exact error probability as given by the Webb simulation as P_e becomes small, but overbounds the simulated error probability by about 0.4 to 0.75 dB at $P_e = 0.02$. On the other hand, the Gaussian approximation, Eq. (13), is quite close to the Webb error probability for larger values of P_e, but diverges from it as P_e becomes smaller. We also observe that the value of P_e below which the Gaussian model fails to be a good approximation decreases as the background photon count $\bar{n}_b$ increases. In Fig. 5 (corresponding to high background-photon levels), the Gaussian approximation tracks the Webb error probability fairly closely over a wide range of P_e values.

[3] Ibid.

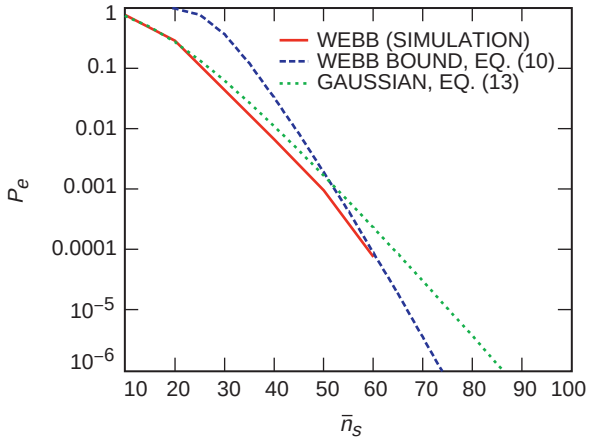

Fig. 1. A comparison of error probabilities using Webb and Gaussian models, $\bar{n}_b = 0.01$, $G = 40.0$.

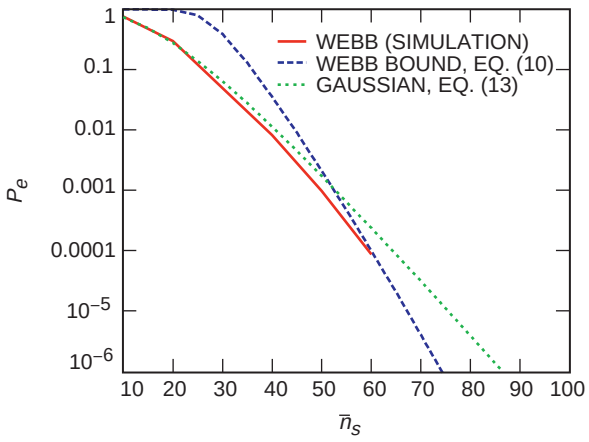

Fig. 2. A comparison of error probabilities using Webb and Gaussian models, $\bar{n}_b = 0.1$, $G = 40.0$.

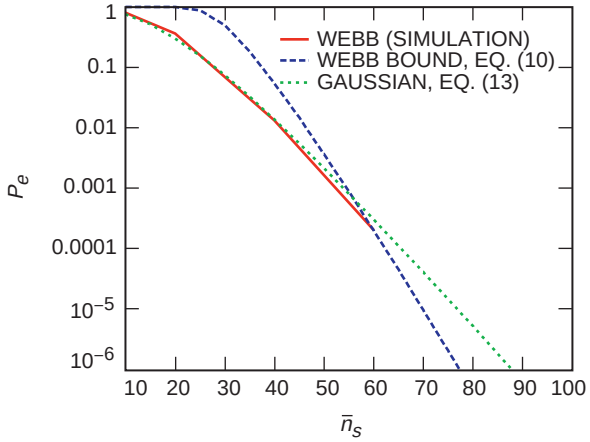

Fig. 3. A comparison of error probabilities using Webb and Gaussian models, $\bar{n}_b = 1$, $G = 40.0$.

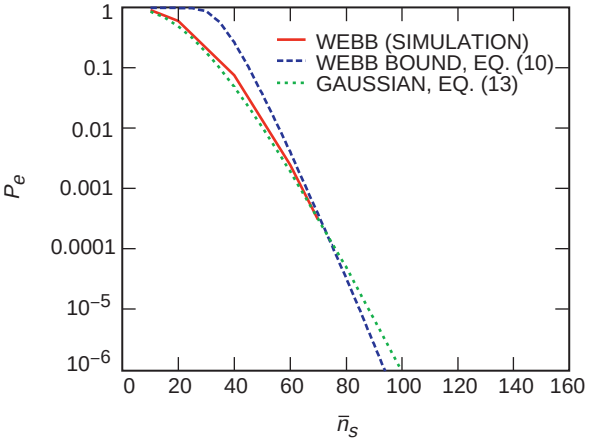

Fig. 4. A comparison of error probabilities using Webb and Gaussian models, $\bar{n}_b = 10$, $G = 40.0$.

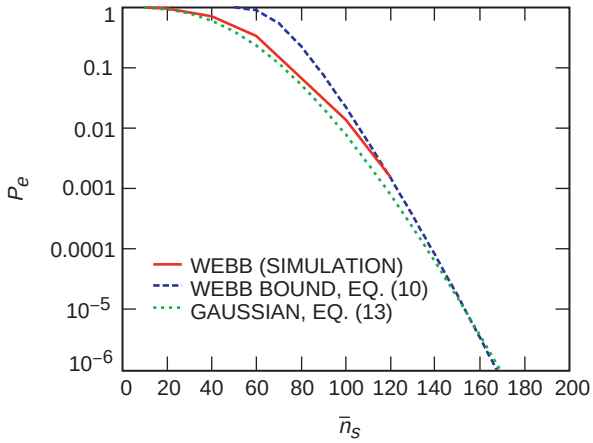

Fig. 5. A comparison of error probabilities using Webb and Gaussian models, $\bar{n}_b = 100$, $G = 40.0$.

In Fig. 6, the results from the previous figures have been compiled to show the number of absorbed signal photons $\bar{n}_s$ that are required in order to achieve fixed PPM symbol-error probabilities of $P_e = 0.02$ and $P_e = 0.002$, as the number of absorbed background photons $\bar{n}_b$ varies. Note that the APD quantum efficiency already has been factored into this figure (as well as the other figures in this article), as given by Eq. (1). In order to obtain the required number of incident signal photons given a certain number of incident background photons, both axes should be scaled by $1/\eta$. In Fig. 6, curves for both the Webb and Gaussian models are shown. We used the results from the Monte Carlo simulations to obtain the curve for the Webb model, since the upper bound is not very tight at $P_e = 0.02$ and $P_e = 0.002$. In Fig. 6, we also plot an approximate analytical expression for the $\bar{n}_s$ versus $\bar{n}_b$ curve that is obtained as follows: By using the Gaussian model for the APD and the union bound on the PPM symbol-error probability, we arrive at

$$P_e \approx \frac{Q-1}{2}\ \mathrm{erfc}\left(\frac{qG\bar{n}_s}{\sqrt{2\left(q^2G^2F(2\bar{n}_b+\bar{n}_s)+2qI_sT_s+\dfrac{4\kappa TT_s}{R}\right)}}\right) \tag{15}$$

Solving for $\bar{n}_s$, we obtain

$$\bar{n}_s \approx A^2F + A\sqrt{A^2F^2 + 4F\bar{n}_b + \frac{4I_sT_s}{qG^2} + \frac{8\kappa TT_s}{q^2G^2R}} \tag{16}$$

where $A = \mathrm{erfc}^{-1}\left([2P_e]/[Q-1]\right)$. We see from Fig. 6 that Expression (16) provides a close approximation to the data for larger values of $\bar{n}_b$ but overestimates $\bar{n}_s$ at small values of $\bar{n}_b$.

In practice, it is possible to tune the APD gain according to the operating conditions in order to achieve improved performance. In our second set of calculations, G was varied for each pair $\{\bar{n}_b, \bar{n}_s\}$

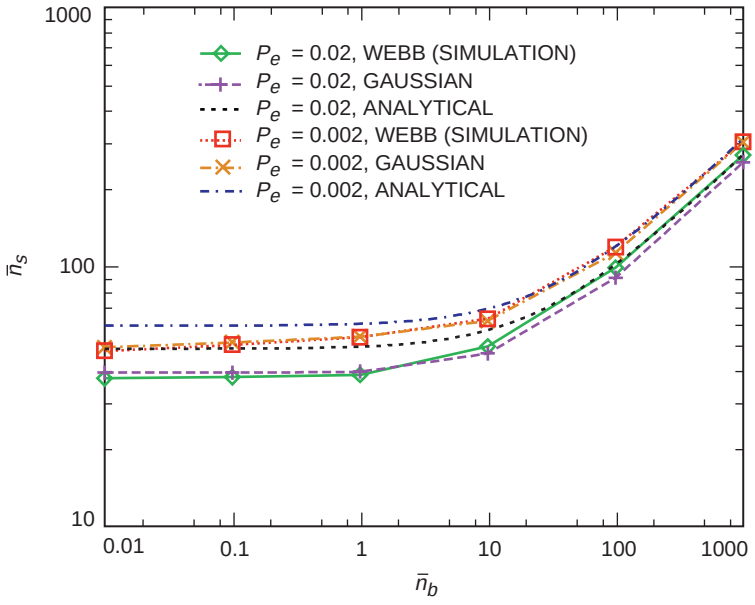

Fig. 6. Plots of $\bar{n}_s$ versus $\bar{n}_b$ at fixed PPM symbol-error probabilities, $G = 40.0$.

in order to obtain the minimum error probability, rather than being held fixed at a particular value. This process is performed for the Webb mixture model and the Gaussian model separately since, for a particular pair $\{\bar{n}_b, \bar{n}_s\}$, the gain that minimizes the symbol-error probability given by the Webb model calculation of Eq. (10) may be different from the gain that minimizes the symbol-error probability given by the Gaussian model calculation of Eq. (13). The Monte Carlo simulation for the Webb model also uses the optimum gain value obtained through minimizing Eq. (10).

Figures 7 through 11 show the resulting graphs of P_e versus $\bar{n}_s$ with optimized G. The most obvious difference between the optimized and fixed-gain results is the improvement in performance around one operating point of interest, $P_e = 0.02$. For fixed gain, this error rate requires $\bar{n}_s = 37, 38, 39, 50$, and 99 (for backgrounds $\bar{n}_b = 0.01, 0.1, 1, 10$, and 100, respectively), whereas for optimized gain, the required average signal count is reduced to $\bar{n}_s = 19, 21, 31, 48$, and 97. Thus, a 3-dB improvement is achieved at the lowest background photon level by adjusting the APD gain. The results shown in Figs. 7 through 11 also differ from the fixed-gain results in that the separation between the Webb and Gaussian models is more pronounced, especially at lower values of $\bar{n}_b$. We see that the Gaussian curve crosses over the Webb curve, so that the Gaussian model underbounds the simulated error probability for smaller values of $\bar{n}_s$ and overbounds the simulated error probability for larger values of $\bar{n}_s$ (although in Figs. 7 and 8 the crossover points are off the scale). The regions of $\bar{n}_s$ in which these two cases occur vary depending on the value of $\bar{n}_b$, with the crossover point increasing as $\bar{n}_b$ increases. Note that in Fig. 7, with $\bar{n}_b = 0.01$, the Gaussian approximation always overbounds the simulated error probability. The upper bound on the Webb error probability, Eq. (10), again is shown to approximate the exact value well as P_e becomes small.

Figure 12 shows the curves of $\bar{n}_s$ versus $\bar{n}_b$ for fixed values of P_e. Comparing Figs. 6 and 12, it may be seen that for high-intensity background levels ($\bar{n}_b \geq 100$), both the optimized and fixed-gain systems require similar levels of average signal photons per pulse in order to achieve a given level of performance. This result also could have been predicted from the fact that the fixed-gain system was optimized for the high-background case. However, for low levels of background radiation, as would be encountered during nighttime operation, the advantage of optimizing the gain clearly is demonstrated. Figure 12 also shows how the Gaussian curve is very close to the Webb curve for high background-photon levels at these error probabilities, but either overbounds or underbounds the Webb results in the other regions. Finally, the gain values that were used in the variable gain calculations are plotted in Fig. 13, which shows the decrease and convergence of optimum gain values as both $\bar{n}_b$ and $\bar{n}_s$ increase.

IV. Conclusions

In this article, we presented performance curves for 256-ary PPM signals received by APD detectors in the presence of Gaussian thermal noise. We compared the performance in terms of PPM symbol-error probability of the Gaussian approximation for APD output electrons to the more accurate Webb model. Although the Gaussian model leads to much simpler analysis and faster calculations, it does not consistently overpredict or underpredict error probability over all regions. This may lead to problems in link analysis when link budgets are tight. On the other hand, using the actual Webb statistics for the APD output modeling results in a complicated mixture process when Gaussian thermal noise is added. The exact symbol-error probability is very difficult and time-consuming to calculate when using this mixture process, thereby necessitating use of an upper bound that does converge to the exact error probability as it becomes smaller. Use of this bound with the Webb model will result in a more consistent prediction of receiver performance, keeping in mind that the bound is pessimistic for larger values of required P_e ($P_e > 0.001$). We also demonstrated through our calculation that, at lower background-photon levels, optimization of APD gain results in significant improvement in receiver performance.

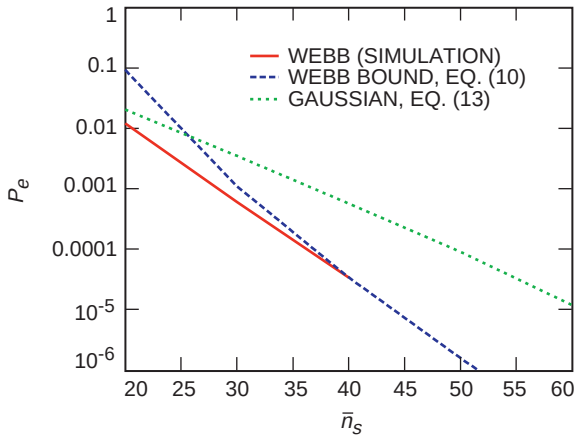

Fig. 7. A comparison of error probabilities using Webb and Gaussian models, $\bar{n}_b$ = 0.01, optimized gain.

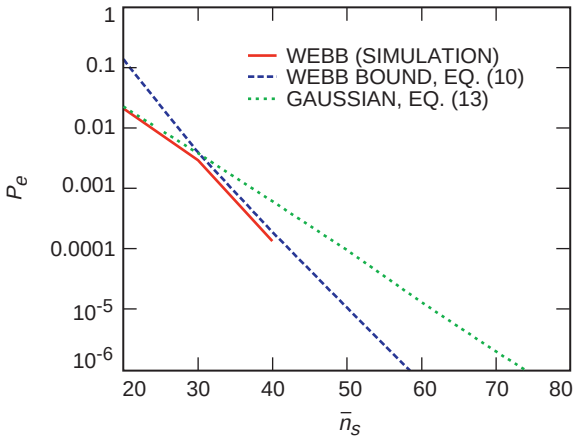

Fig. 8. A comparison of error probabilities using Webb and Gaussian models, $\bar{n}_b$ = 0.1, optimized gain.

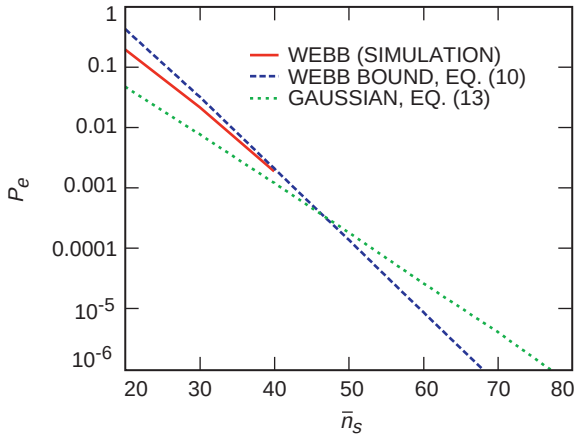

Fig. 9. A comparison of error probabilities using Webb and Gaussian models, $\bar{n}_b$ = 1, optimized gain.

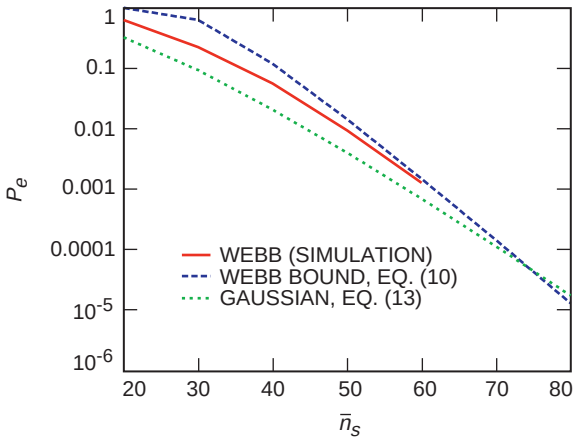

Fig. 10. A comparison of error probabilities using Webb and Gaussian models, $\bar{n}_b$ = 10, optimized gain.

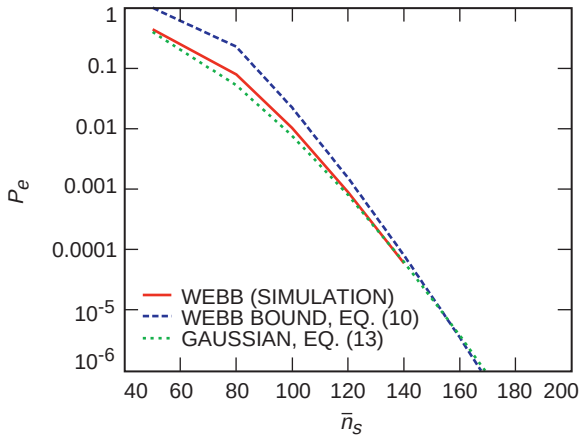

Fig. 11. A comparison of error probabilities using Webb and Gaussian models, $\bar{n}_b$ = 100, optimized gain.

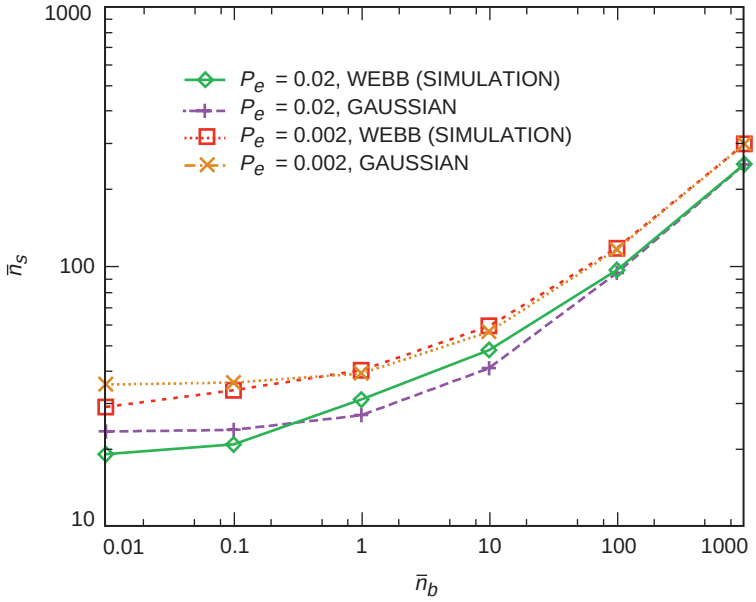

Fig. 12. Plots of $\bar{n}_s$ versus $\bar{n}_b$ at fixed PPM symbol-error probabilities, with optimized gain.

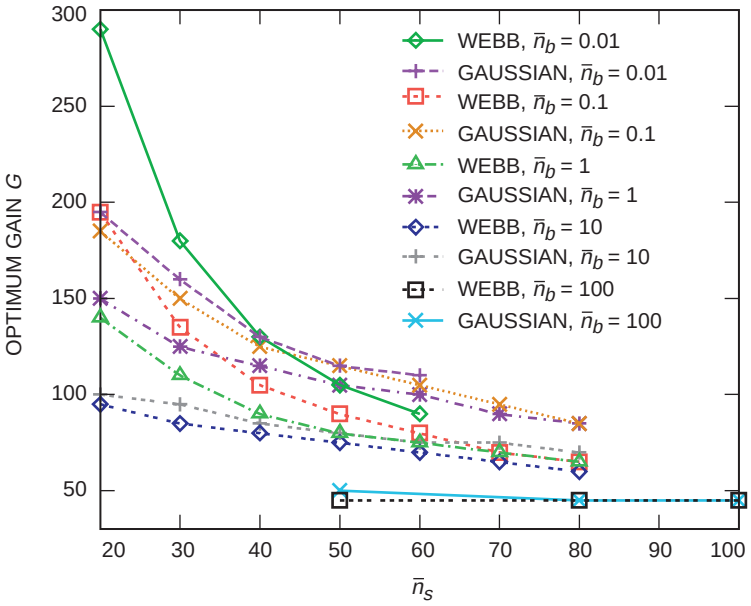

Fig. 13. Optimum gain values using Webb and Gaussian models.

Acknowledgments

The authors acknowledge Chien Chen, Marvin Simon, and Tsun-Yee Yan for valuable discussions on the material presented here.

References

[1] R. J. McIntyre, "The Distribution of Gains in Uniformly Multiplying Avalanche Photodiodes: Theory," *IEEE Transactions on Electron Devices*, vol. ED-19, no. 6, pp. 703–713, June 1972.

[2] J. Conradi, "The Distribution of Gains in Uniformly Multiplying Avalanche Photodiodes: Experimental," *IEEE Transactions on Electron Devices*, vol. ED-19, no. 6, pp. 713–718, June 1972.

[3] F. M. Davidson and X. Sun, "Gaussian Approximation Versus Nearly Exact Performance Analysis of Optical Communications Systems With PPM Signaling and APD Receivers," *IEEE Transactions on Communications*, vol. 36, no. 11, pp. 1185–1192, November 1988.

[4] P. P. Webb, R. J. McIntyre, and J. Conradi, "Properties of Avalanche Photodiodes," *RCA Review*, vol. 35, pp. 234–278, June 1974.

[5] M. Srinivasan and V. Vilnrotter, "Performance of the Optimum Receiver for Pulse-Position Modulation Signals With Avalanche Photodiode Statistics," *The Telecommunications and Mission Operations Progress Report 42-133, January–March 1998*, Jet Propulsion Laboratory, Pasadena, California, pp. 1–10, May 15, 1998.
http://tmo.jpl.nasa.gov/tmo/progress_report/42-133/133H.pdf

[6] V. Vilnrotter, M. Simon, and M. Srinivasan, *Maximum Likelihood Detection of PPM Signals Governed by an Arbitrary Point Process Plus Additive Gaussian Noise*, JPL Publication 98-7, Jet Propulsion Laboratory, Pasadena, California, April 1998.

[7] L. Hughes, "A Simple Upper Bound on the Error Probability for Orthogonal Signals in White Noise," *IEEE Transactions on Communications*, vol. COM-40, no. 4, p. 670, April 1992.

[8] W. H. Press, W. T. Vetterling, S. A. Teukolsky, and B. P. Flannery, *Numerical Recipes in C*, New York: Cambridge University Press, 1992.

[9] J. K. Townsend and K. S. Shanmugan, "On Improving the Computational Efficiency of Digital Lightwave Link Simulation," *IEEE Transactions on Communications*, vol. 38, no. 11, November 1990.